JACS
JOURNAL OF THE AMERICAN CHEMICAL SOCIETY

Communication

pubs.acs.org/JACS

Anisotropic Nanoparticles as Shape-Directing Catalysts for the Chemical Etching of Silicon

Guoliang Liu,[†] Kaylie L. Young,[†] Xing Liao,[‡] Michelle L. Personick,[†] and Chad A. Mirkin*[,†,‡]

[†]Department of Chemistry and International Institute for Nanotechnology and [‡]Department of Materials Science and Engineering, Northwestern University, 2145 Sheridan Road, Evanston, Illinois 60208, United States

Supporting Information

ABSTRACT: Anisotropic Au nanoparticles have been used to create a library of complex features on silicon surfaces. The technique provides control over feature size, shape, and depth. Moreover, a detailed study of the etching rate as a function of the nanoparticle surface facet interfaced with the silicon substrate suggested that the etching is highly dependent upon the facet surface energy. Specifically, the etching rate for Au nanocubes with {100}-terminated facets was ~1.5 times higher than that for triangular nanoprisms with {111} facets. Furthermore, this work gives fundamental insight into the mechanism of metal-catalyzed chemical etching.

Fabrication of silicon nanostructures is central to many processes in a variety of fields and applications, including microelectronics,[1] sensing,[2] information storage,[3] photonics,[4] photovoltaics,[5] and energy storage.[6] Compared with conventional dry-etching methods such as reactive ion etching, metal-assisted chemical etching does not involve reactive ions and offers numerous advantages such as minimal ion-induced doping on the silicon sidewalls, the ability to fabricate features with high aspect ratios, and significantly lower cost. Despite the great potential of metal-assisted chemical etching techniques, the metal films that are used as templates for etching often have poor crystallinity, resulting in lack of control over the feature shape, uniformity, and etching direction.[7] Moreover, because of the complicated etching chemistry, the mechanism is still subject to debate.[7] In this work, we utilized a variety of crystalline nanoparticles, enabled by recent developments in scanning probe block-copolymer lithography (SPBCL)[8,9] and anisotropic nanoparticle synthesis,[10−13] to create a library of complex silicon features based upon metal-assisted chemical etching. The anisotropic nanoparticles provided a unique opportunity to investigate the role of surface facets in the etching mechanism. By comparing the etching rates for different nanoparticle surface facets interfaced with the underlying Si substrate, we were able to rule out one of the two debated etching mechanisms in the literature and in the process provide greater insight into the chemistry underlying this metal-catalyzed chemical reaction.

With current metal-assisted chemical etching processes, the metal templates are often made by thermal evaporation,[14] sputtering,[15] electron beam evaporation,[16] electroless deposition,[17] electrode deposition,[18] or focused-ion-beam deposition techniques.[19] These methods typically generate polycrystalline structures with impurities and defects that result in unpredictable etching behavior.[7] The lack of crystallinity in such structures hinders not only control over the nanoscale features but also attempts to understand the fundamental chemical etching process.[20] Colloidal nanoparticles, particularly those composed of noble metals such as Au, Ag, Pt, and Pd, can be synthesized with a wide range of sizes and shapes, and more importantly, with a high degree of crystallinity.[10−13] While these nanoparticles are now the basis for a wide variety of functional materials and devices, including superlattices,[21,22] chemical and biological sensors,[23] imaging agents,[23] plasmonic entities,[23,24] and catalysts,[25] they have never been explored as templates for chemical etching to create nanostructures with well-defined geometric dimensions. The high degree of crystallinity and almost atomically flat surface facets[26] of anisotropic nanoparticles can potentially result in extremely uniform etching profiles in the underlying substrate, affording unprecedented control over the etched structure shape and dimensions, including line edge roughness. In addition, from a fundamental perspective, the reactivity can depend on the exposed surfaces of the nanoparticles. Therefore, these crystalline nanoparticles provide an unusual opportunity to investigate the role of surface facets on chemical etching, which is impossible with conventionally deposited metal films.[7]

The etching of silicon occurs via the chemical reaction[7]

$$\mathrm{Si} + \mathrm{H_2O_2} + 6\mathrm{HF} \xrightarrow{\mathrm{Au}} 2\mathrm{H_2O} + \mathrm{H_2SiF_6} + \mathrm{H_2}$$

and the etching process consists of three steps: deposition of Au nanoparticles, chemical etching with HF/H_2O_2, and dissolution of the nanoparticles with aqua regia (Figure 1). As a proof of concept, spherical nanoparticles were first used as templates to etch patterned arrays of silicon nanopores. Utilizing our recently developed SPBCL technique, which provides the ability to synthesize nanoparticles site-specifically with control over the diameter at the single-nanoparticle level,[8,9] we prepared a library of particles of predesignated sizes in the 4.0 to 25.5 nm range (Figure 2 and Figure S1 in the Supporting Information). Because a high-temperature (500 °C) annealing step is used in the SPBCL process, the nanoparticles exhibit a high degree of crystallinity.[8,27] It is worth noting that SPBCL is a high-throughput method that can be used to synthesize nanoparticle arrays over centimeter-scale areas. A comparison of magnified views of a 2 × 2 Au nanoparticle array

Received: June 20, 2013
Published: August 1, 2013

   dx.doi.org/10.1021/ja4061867 | J. Am. Chem. Soc. 2013, 135, 12196−12199

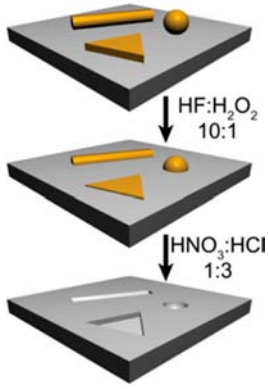

Figure 1. Schematic of metal-assisted chemical etching using crystalline gold nanoparticles.

before and after chemical etching (Figure S1) showed that the etching yielded nanopores with a diameter slightly larger than that of the nanoparticles.

The diameter of the nanopores could be controlled by changing the nanoparticle size. The diameter of the nanoparticles was deliberately adjusted in a tightly controlled fashion by changing the amount of metal ion precursor that was patterned on the substrate during SPBCL (Figure 2 top).

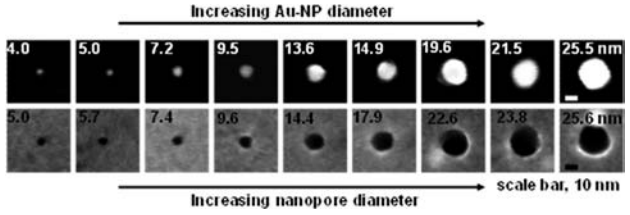

Figure 2. Scanning electron microscopy (SEM) images of (top) gold nanoparticles with various diameters and (bottom) the corresponding silicon nanopores formed by metal-assisted chemical etching. The gold nanoparticles were removed by immersing the substrate with the nanoparticles in aqua regia.

During chemical etching, the nanoparticles catalyzed the dissolution of the underlying silicon, resulting in corresponding nanopores with diameters ranging from 5.0 to 25.6 nm (Figure 2 bottom). The nanoparticles could be used to create comparably sized nanopores in the silicon after chemical etching, indicating that the diameter of the nanopores is dictated by the diameter of the Au nanoparticles.

Interestingly, as the nanoparticle size increased, the particles started to develop facets, and the resulting etched features also exhibited facets (a pentatwinned silicon feature is shown in Figure S2). Inspired by such behavior, we continued to explore the potential of utilizing anisotropic nanoparticles such as nanorods,[28] nanocubes,[11] and nanoplates,[29,30] which have well-defined facets, as catalysts to etch features with various projected shapes, including lines, squares, triangles, trapezoids, and hexagons (Figure 3). Nanorods with aspect ratios of 25 [length (L) = 726 nm, diameter (d) = 29 nm] and 5.3 (L = 59.4 nm, d = 11.3 nm) were used to make trenched features, demonstrating the ability to use nanorods to create linear features in a silicon substrate. Because the high-aspect-ratio nanorods had almost atomically smooth edges,[26] the etched lines were remarkably straight. Similarly, Au nanoprisms are nanoparticles with atomically flat {111} top and bottom basal

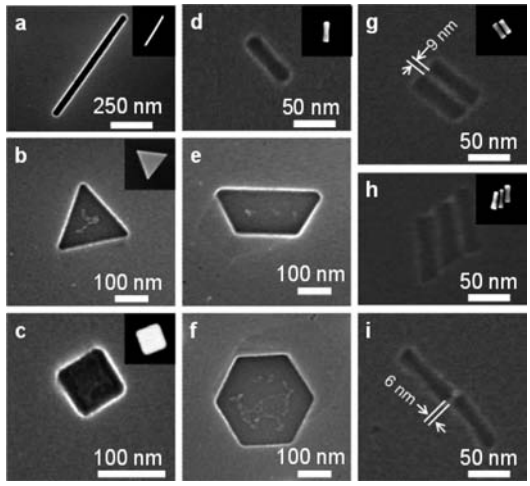

Figure 3. SEM images of complex features etched into silicon using anisotropic Au nanoparticles as templates. The insets show the corresponding nanoparticles before etching. With clusters of particles (g–i), 9 nm wide silicon walls formed between rods that were aligned side-by-side along their long axes (g, h), while for rods adjacent to one another in an end-on fashion, a 6 nm feature separated the recessed structures (i). The gray patches inside the broad features in (b), (c), (e), and (f) are attributed to ligand residue but were not chemically characterized.

surfaces.[31] Trapezoid- and hexagon-shaped nanoplates are of the same family. Complex geometries with various projected shapes such as triangles, trapezoids, and hexagons were etched using these nanoparticles. Lastly, nanocubes, which possess atomically flat {100} surface facets, were used to etch square-shaped features in silicon. While individual nanoparticles could be used as templates for a wide variety of shapes, assembled nanoparticles could be employed to create wall-like features between etched troughs (Figure 3g–i). It should be noted that such silicon walls and bridges are important features in microelectronic devices.[1]

These anisotropic nanoparticles have highly faceted surfaces that are not present in metal films formed from deposition or evaporation,[14−19] providing an opportunity to investigate the effect of the crystal facet on chemical etching. Au triangular nanoprisms with {111} surface facets and nanocubes with {100} surface facets were placed on the same substrate, immersed in the same solution, and etched for 20 min. As measured by atomic force microscopy (AFM), the thickness of the nanoprism and the edge length of the nanocube were 6.9 and 112.0 nm, respectively. The etched silicon features were characterized by both AFM and SEM (Figure 4). The AFM line scans showed that nanocubes with {100} facets exhibited a higher etching rate than nanoprisms with {111} facets, as the etched depths after 20 min of immersion were 48.6 and 31.8 nm, respectively. The different etching rates can be explained by the different shapes of the nanoparticles, which result in different surface facets being placed in direct contact with the underlying silicon substrate. The higher surface energy of {100} facets relative to {111} facets results in higher catalytic activity and easier hole injection into silicon for the oxidation reaction (Figure 5), leading to a higher silicon etching rate.[32] More compellingly, our hypothesis that the etching rate is related to the metal surface energy (γ) is also in line with the reported etching rates for different metals,[33] which increase with increasing γ [Ag (γ = 1.246−1.250 J m^{-2}) < Au (γ = 1.500−

dx.doi.org/10.1021/ja4061867 | J. Am. Chem. Soc. 2013, 135, 12196−12199

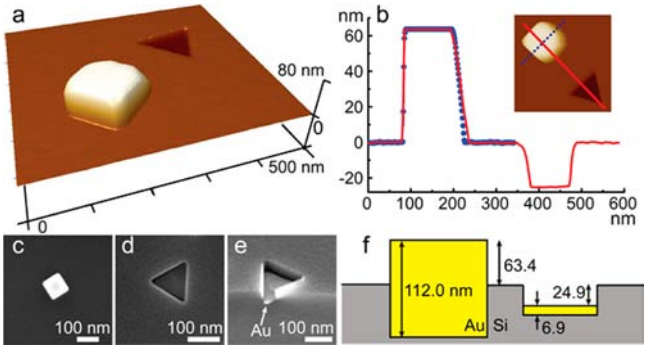

Figure 4. (a) AFM height images of a Au nanocube and a Au nanoprism on a silicon substrate after etching for 20 min. Part of the cube is above the surface, while the entire nanoprism is within the etched triangular trench in the silicon substrate. (b) AFM height profiles of the etched features. The inset shows the direction of the line scans. (c, d) Top-down SEM images of (c) a nanocube and (d) a nanoprism after etching for 20 min. (e) SEM cross-sectional view of a nanoprism in a silicon trench at a 45° tilt angle. (f) Schematic side view of the etching depths obtained using a nanocube (yellow square) and a nanoprism (yellow rectangle). All of the labeled distances are in nanometers, as measured by AFM. For clarity, the schematic is not drawn to scale.

1.506 J m^{-2}) < Pt (γ = 2.475–2.489 J m^{-2}) < Rh (γ = 2.659–2.700 J m^{-2})].[32]

The chemical reaction catalyzed by crystalline nanoparticles can also give insight into the etching mechanism. There are two proposed models for metal-assisted chemical etching, yet to date there is no direct evidence in the literature to prove or disprove either one.[7] In model I, Si atoms are oxidized at the bottom surface of the metal and then diffuse along the metal–Si interface to the bulk solution (Figure 5 left);[17,34] in model II,

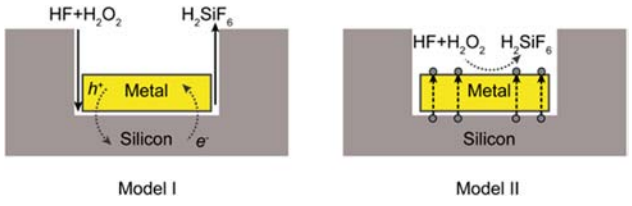

Figure 5. Schematics of the two models for metal-assisted chemical etching. The redox reaction occurs at the metal–Si interface (i.e., the bottom surface of metal) in model I and at the metal–solution interface (i.e., the top surface of metal) in model II.

Si atoms dissolve in the metal, diffuse across the metal lattice, and then are oxidized at the top surface[7,35,36] (Figure 5 right). The observations in this report are at odds with model II for two reasons. First, because of the high surface energy at their sharp tips, triangular nanoprisms are not the most energetically favorable structure and are susceptible to shape rearrangement (Figure S3). If model II applies, the dissolved Si should disrupt the original lattice defining the Au prisms and reshape the prisms to more energetically favorable rounded disks or spheres. Our data show that the prisms maintained their original shape throughout the etching process (Figure 3 and 4). Second, if Si atoms diffuse across the metal and oxidize at the top surface, the 112 nm thick Au nanocubes should have a much lower etching rate than the 6.9 nm thick Au nanoprisms because of the order of magnitude longer diffusion length. However, our data show the reverse. These observations rule out the argument in model II that Si dissolves in Au nanoparticles. On the contrary, the slightly larger diameter of the etched silicon features compared with that of the nanoparticles (Figure 2) indicates a favorable diffusion channel for the reactants/products between the metal and Si, suggesting that model I is a more plausible mechanism for metal-assisted chemical etching. In contrast with a previous report,[37] where the reagents appeared to diffuse in a porous silicon layer, there was no apparent porous layer beneath the etched trenches (Figures 4e and S4), consistent with the notion that a porous silicon layer is not a necessity in metal-assisted chemical etching and the reactants/products can diffuse along the metal–Si interface. With a longer etching time, a porous layer slowly developed on the sidewalls of deeper trenches and the top surface of the silicon substrate (Figure S4 and S5),[38] following the well-known porous silicon formation mechanism.[39]

In summary, we have studied Au-nanoparticle-catalyzed chemical etching of silicon and shown that anisotropic nanoparticles can be used to create nanostructures with control over the feature size and shape. The well-defined surface facets of anisotropic nanoparticles allowed us to investigate the difference in etching rates between Au {100} and {111} surfaces and provide fundamental insight into the chemical etching mechanism. Looking forward, the silicon nanostructures resulting from this method could be used as topographic templates for the assembly and positioning of smaller nanoparticles. In addition, when coupled with emerging high-resolution, large-area scanning probe lithography methods,[40–42] this technique should provide access to a variety of nanofeatures essential for semiconductor, nanofluidic, and magnetic data storage devices.[1,3,43]

■ ASSOCIATED CONTENT

Supporting Information

Procedures and characterization data. This material is available free of charge via the Internet at http://pubs.acs.org.

■ AUTHOR INFORMATION

Corresponding Author

chadnano@northwestern.edu

Notes

The authors declare no competing financial interest.

■ ACKNOWLEDGMENTS

This material is based upon work supported by the following awards: AFOSR FA9550-09-1-0294, DoD/NSSEFF Program/NPS N00244-09-1-0012 and N00244-09-1-0071, NSF MRSEC DMR-1121262, DARPA/MTO HR0011-13-2-0002, and NERC/DoE DE-SC0000989. K.L.Y. gratefully acknowledges support from the National Science Foundation and a National Defense Science and Engineering Graduate Research Fellowship. X.L. gratefully acknowledges support through a Ryan Fellowship. M.L.P. gratefully acknowledges support from the NSF through the Graduate Research Fellowship Program (GRFP).

■ REFERENCES

(1) Black, C. T.; Ruiz, R.; Breyta, G.; Cheng, J. Y.; Colburn, M. E.; Guarini, K. W.; Kim, H. C.; Zhang, Y. *IBM J. Res. Dev.* **2007**, *51*, 605.
(2) Jeon, H. C.; Heo, C. J.; Lee, S. Y.; Yang, S. M. *Adv. Funct. Mater.* **2012**, *22*, 4268.
(3) Albrecht, T. R.; Bedau, D.; Dobisz, E.; Gao, H.; Grobis, M.; Hellwig, O.; Kercher, D.; Lille, J.; Marinero, E.; Patel, K.; Ruiz, R.;

Schabes, M. E.; Wan, L.; Weller, D.; Wu, T.-W. *IEEE Trans. Magn.* **2013**, *49*, 773.
(4) Tolmachev, V. A.; Astrova, E. V.; Pilyugina, J. A.; Perova, T. S.; Moore, R. A.; Vij, J. K. *Opt. Mater.* **2005**, *27*, 831.
(5) Li, X. L. *Curr. Opin. Solid State Mater. Sci.* **2012**, *16*, 71.
(6) Lin, C. C.; Yen, Y. C.; Wu, H. C.; Wu, N. L. *J. Chin. Chem. Soc.* **2012**, *59*, 1226.
(7) Huang, Z.; Geyer, N.; Werner, P.; de Boor, J.; Gösele, U. *Adv. Mater.* **2011**, *23*, 285.
(8) Liu, G.; Eichelsdoerfer, D. J.; Rasin, B.; Zhou, Y.; Brown, K. A.; Liao, X.; Mirkin, C. A. *Proc. Natl. Acad. Sci. U.S.A.* **2013**, *110*, 887.
(9) Chai, J.; Huo, F.; Zheng, Z.; Giam, L. R.; Shim, W.; Mirkin, C. A. *Proc. Natl. Acad. Sci. U.S.A.* **2010**, *107*, 20202.
(10) Xia, Y.; Xiong, Y.; Lim, B.; Skrabalak, S. E. *Angew. Chem., Int. Ed.* **2009**, *48*, 60.
(11) Langille, M. R.; Personick, M. L.; Zhang, J.; Mirkin, C. A. *J. Am. Chem. Soc.* **2012**, *134*, 14542.
(12) Personick, M. L.; Langille, M. R.; Zhang, J.; Mirkin, C. A. *Nano Lett.* **2011**, *11*, 3394.
(13) Sun, Y.; Xia, Y. *Science* **2002**, *298*, 2176.
(14) Hui, F.; Yin, W.; Jiahao, Z.; Jing, Z. *Nanotechnology* **2006**, *17*, 3768.
(15) Huang, Z.; Zhang, X.; Reiche, M.; Liu, L.; Lee, W.; Shimizu, T.; Senz, S.; Gösele, U. *Nano Lett.* **2008**, *8*, 3046.
(16) Chang, S.-W.; Chuang, V. P.; Boles, S. T.; Ross, C. A.; Thompson, C. V. *Adv. Funct. Mater.* **2009**, *19*, 2495.
(17) Peng, K.; Wu, Y.; Fang, H.; Zhong, X.; Xu, Y.; Zhu, J. *Angew. Chem., Int. Ed.* **2005**, *44*, 2737.
(18) Yae, S.; Kawamoto, Y.; Tanaka, H.; Fukumuro, N.; Matsuda, H. *Electrochem. Commun.* **2003**, *5*, 632.
(19) Chattopadhyay, S.; Bohn, P. W. *J. Appl. Phys.* **2004**, *96*, 6888.
(20) Tsujino, K.; Matsumura, M. *Electrochim. Acta* **2007**, *53*, 28.
(21) Park, S. Y.; Lytton-Jean, A. K. R.; Lee, B.; Weigand, S.; Schatz, G. C.; Mirkin, C. A. *Nature* **2008**, *451*, 553.
(22) Murray, C. B.; Kagan, C. R.; Bawendi, M. G. *Annu. Rev. Mater. Sci.* **2000**, *30*, 545.
(23) Lee, K.-S.; El-Sayed, M. A. *J. Phys. Chem. B* **2006**, *110*, 19220.
(24) Lu, X.; Rycenga, M.; Skrabalak, S. E.; Wiley, B.; Xia, Y. *Annu. Rev. Phys. Chem.* **2009**, *60*, 167.
(25) Lim, B.; Jiang, M.; Camargo, P. H. C.; Cho, E. C.; Tao, J.; Lu, X.; Zhu, Y.; Xia, Y. *Science* **2009**, *324*, 1302.
(26) Goris, B.; Bals, S.; Van den Broek, W.; Carbó-Argibay, E.; Gómez-Graña, S.; Liz-Marzán, L. M.; Van Tendeloo, G. *Nat. Mater.* **2012**, *11*, 930.
(27) Liu, G.; Zhou, Y.; Banga, R. S.; Boya, R.; Brown, K. A.; Chipre, A. J.; Nguyen, S. T.; Mirkin, C. A. *Chem. Sci.* **2013**, *4*, 2093.
(28) Jana, N. R.; Gearheart, L.; Murphy, C. J. *J. Phys. Chem. B* **2001**, *105*, 4065.
(29) Young, K. L.; Jones, M. R.; Zhang, J.; Macfarlane, R. J.; Esquivel-Sirvent, R.; Nap, R. J.; Wu, J. S.; Schatz, G. C.; Lee, B.; Mirkin, C. A. *Proc. Natl. Acad. Sci. U.S.A.* **2012**, *109*, 2240.
(30) Millstone, J. E.; Wei, W.; Jones, M. R.; Yoo, H. J.; Mirkin, C. A. *Nano Lett.* **2008**, *8*, 2526.
(31) Millstone, J. E.; Park, S.; Shuford, K. L.; Qin, L.; Schatz, G. C.; Mirkin, C. A. *J. Am. Chem. Soc.* **2005**, *127*, 5312.
(32) Vitos, L.; Ruban, A. V.; Skriver, H. L.; Kollar, J. *Surf. Sci.* **1998**, *411*, 186.
(33) Yae, S.; Morii, Y.; Fukumuro, N.; Matsuda, H. *Nanoscale Res. Lett.* **2012**, *7*, 1.
(34) Peng, K. Q.; Hu, J. J.; Yan, Y. J.; Wu, Y.; Fang, H.; Xu, Y.; Lee, S. T.; Zhu, J. *Adv. Funct. Mater.* **2006**, *16*, 387.
(35) Hiraki, A.; Nicolet, M. A.; Mayer, J. W. *Appl. Phys. Lett.* **1971**, *18*, 178.
(36) Xie, T.; Schmidt, V.; Pippel, E.; Senz, S.; Gösele, U. *Small* **2008**, *4*, 64.
(37) Geyer, N.; Fuhrmann, B.; Huang, Z.; de Boor, J.; Leipner, H. S.; Werner, P. *J. Phys. Chem. C* **2012**, *116*, 13446.
(38) Smith, Z. R.; Smith, R. L.; Collins, S. D. *Electrochim. Acta* **2013**, *92*, 139.
(39) Zhang, X. G. *J. Electrochem. Soc.* **2004**, *151*, C69.
(40) Huo, F. W.; Zheng, Z. J.; Zheng, G. F.; Giam, L. R.; Zhang, H.; Mirkin, C. A. *Science* **2008**, *321*, 1658.
(41) Huo, F.; Zheng, G.; Liao, X.; Giam, L. R.; Chai, J.; Chen, X.; Shim, W.; Mirkin, C. A. *Nat. Nanotechnol.* **2010**, *5*, 637.
(42) Shim, W.; Braunschweig, A. B.; Liao, X.; Chai, J. N.; Lim, J. K.; Zheng, G. F.; Mirkin, C. A. *Nature* **2011**, *469*, 516.
(43) Liu, G. L.; Thomas, C. S.; Craig, G. S. W.; Nealey, P. F. *Adv. Funct. Mater.* **2010**, *20*, 1251.